Three-Dimensional Structures of MoS_2 Nanosheets with Ultrahigh Hydrogen Evolution Reaction in Water Reduction

Xiumei Geng, Wei Wu, Ning Li, Weiwei Sun, Johnathan Armstrong, Alaa Al-hilo, Matthew Brozak, Jingbiao Cui, and Tar-pin Chen**

The hydrogen evolution reaction in an alkaline environment using a non-precious catalyst with much greater efficiency represents a critical challenge in research. Here, a robust and highly active system for hydrogen evolution reaction in alkaline solution is reported by developing MoS_2 nanosheet arrays vertically aligned on graphene-mediated 3D Ni networks. The catalytic activity of the 3D MoS_2 nanostructures is found to increase by 2 orders of magnitude as compared to the Ni networks without MoS_2. The MoS_2 nanosheets vertically grow on the surface of graphene by employing tetrakis(diethylam inodithiocarbomato)molybdate(IV) as the molybdenum and sulfur source in a chemical vapor deposition process. The few-layer MoS_2 nanosheets on 3D graphene/nickel structure can maximize the exposure of their edge sites at the atomic scale and present a superior catalysis activity for hydrogen production. In addition, the backbone structure facilitates as an excellent electrode for charge transport. This precious-metal-free and highly efficient active system enables prospective opportunities for using alkaline solution in industrial applications.

1. Introduction

Electrocatalysis plays a pivotal role in renewable energy technology, especially in hydrogen evolution reaction (HER) for water splitting.[1,2] HER is a fundamental electrochemical reaction to explore electrode stability, catalysis kinetics and basic reaction mechanism of converting protons (acid) or water (alkaline) into molecular hydrogen. Most HER catalyst activity in acid medium is superior to that in alkaline medium by ~2 to 3 orders of magnitude.[3,4] The current dilemma for HER in alkaline medium mainly lies in sluggish kinetics and unacceptable high cost of precious metal. Development of excellent catalytic activity with high stability and cost-effective catalysts is of great importance in improving HER performance in alkaline medium.

Precious metal Pt,[5–7] precious metal (Pt, Ir, Ru) modified on porous substrates[8–11] and other metal alloy[12–16] have been used as catalysts in alkaline medium. These catalysts showed reasonable cathode current density for HER. Studies to improve catalyst kinetics by modifying or introducing other compounds have also been reported. So far, the best result on Pt catalyst system in alkaline medium achieved by tailoring Li^+-$Ni(OH)_2$-Pt interface has shown 10 times improvement in activity as compared to metal Pt catalyst alone.[17] However, the high cost of Pt hinders its extensive commercial applications. High surface-area Raney Ni and Ni alloy are actually used to serve as a catalyst in conventional water alkaline electrolyzers.[18,19] Although efforts have been made towards higher catalyst loading,[15] or change in the alloy composition for improving Ni or its alloy catalyst system, it has not changed the fact that its catalyst activity still remains sluggish and at a relatively low level. If this bottleneck on Ni catalyst system can be eliminated, the remarkable efficiency improvement in HER and substantial electrical energy saving will become possible in hydrogen production. Indeed, by modifying $Ni(OH)_2$ nanoclusters on a Ni electrode, the HER is four times higher than that using unmodified Ni.[20]

Due to its capability in effectively cleaving the HO–H bond,[21,22] MoS_2, a two-dimensional layered materials, has been recognized as one of the important materials for low cost HER with high photocatalytic and electrocatalytic efficiency. Its nanometer-scale edges have been theoretically and experimentally proved to be active sites for HER.[23–28] Maximizing the number of exposed edge site can strikingly boost the catalytic activity. Many methods have been used to increase the exposure of the edge sites, which include growth of MoS_2 vertically on flat substrate and synthesis of MoS_2 vertically on curved and rough nanowire surfaces.[29,30] Three dimensional (3D) MoS_2 structures have also been fabricated to maximize the density of active catalytic sites, however, poor electric and mass transport limit their catalytic efficiency.[31] Amorphous MoS_x ($x \geq 2$) on graphene-coated Ni foam showed advantages on HER in acid solution due to improved catalyst

Dr. X. Geng, W. Wu, W. Sun, J. Armstrong, A. Al-hilo, M. Brozak, Prof. T.-P.Chen
Department of Physics and Astronomy
University of Arkansas at Little Rock
Arkansas 72204, USA
E-mail: txchen@ualr.edu
Dr. N. Li
Center for Cancer and Immunology Research
Children's National Medical Center
Washington DC 20010, USA
Prof. J. Cui
Department of Physics
University of Memphis
Tennessee 38152, USA
E-mail: jcui@memphis.edu

DOI: 10.1002/adfm.201401328

loading. Unfortunately, Ni foam is unstable in acid solution.[32] To our knowledge, highly efficient and cost-effective precious-metal free catalyst for water splitting in alkaline solution has not been developed so far. We report here for the first time a robust and highly active system for hydrogen evolution reaction in alkaline solution using 3D MoS_2 structures composed of vertically aligned nanosheet arrays on the surface of graphene-mediated 3D Ni networks. The catalytic activity from the 3D structure was found to increase by 2 orders of magnitude than the Ni backbone without MoS_2.

2. Results and Discussion

The 3D MoS_2 nanosheets (3D MoS_2-G-Ni) structure was synthesized by employing tetrakis(diethylaminodithiocarbomato) molybdate(IV)[33] as both the molybdenum and sulfur source in a chemical vapor deposition (CVD) process as schematically illustrated in **Figure 1**a. First, graphene was grown on the 3D Ni foam surface by CVD (see the Supporting Information for experimental details) to form the 3D G-Ni structure. High resolution transmission electron microscopy (HRTEM) was used to examine the crystallinity and layer number of graphene. Few-layer and multi-layer were confirmed as shown in Figure 1b and 1c. The samples were prepared by dissolving Ni completely in $FeCl_3$ solution for 2 days. The graphene foam was cleaned by DI water and sonicated for 5 minutes in ethanol. Selected area electron diffraction (SAED) (Figure 1d) demonstrates a good crystallinity of graphene from the area in Figure S1. Four (Figure 1b) and 15 layers (Figure 1c) of graphene were obtained, depending on the catalyst thickness of Ni at different zone in the three dimensional Ni foam. A long growth time of

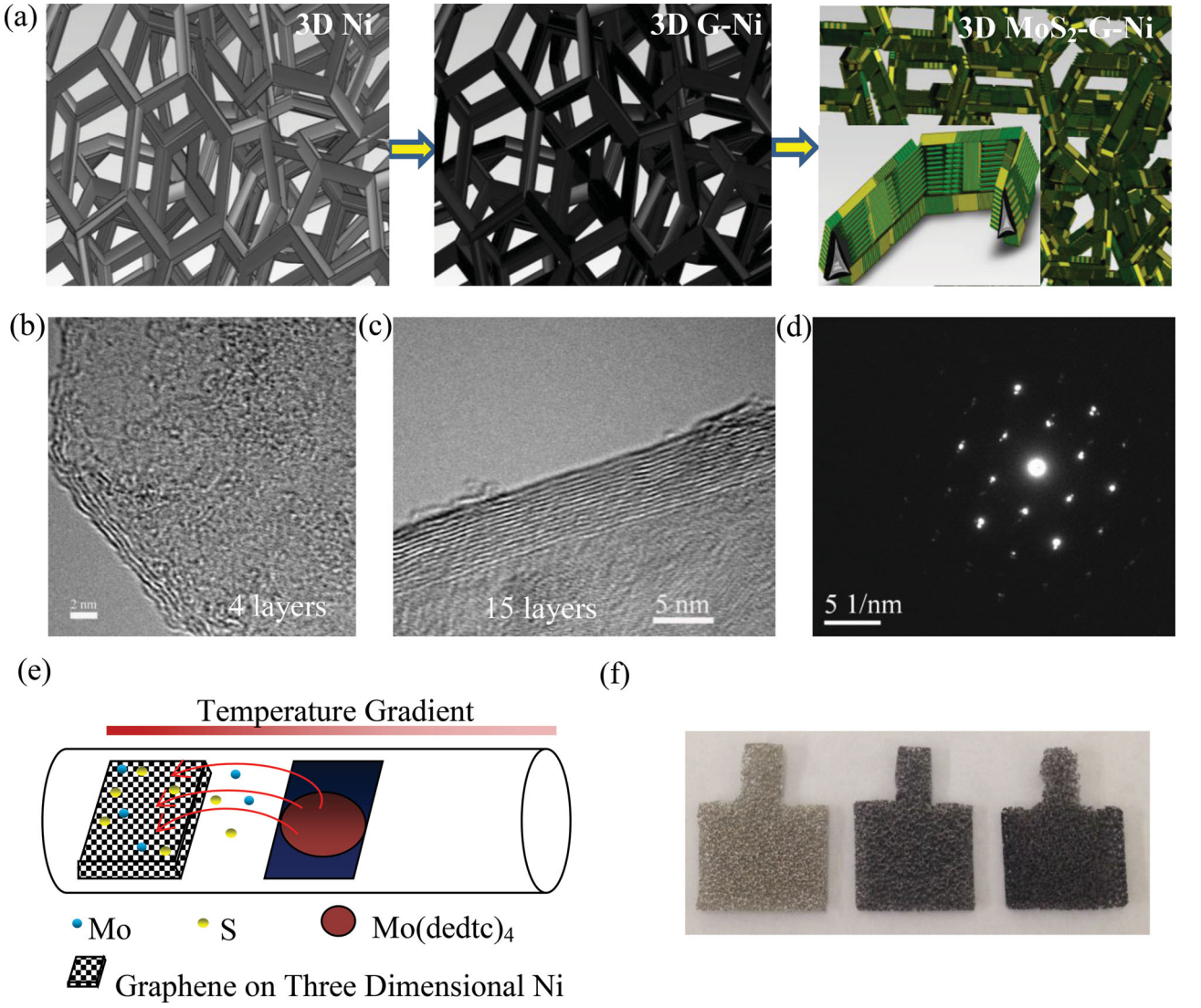

Figure 1. Fabrication of 3D MoS_2-G-Ni structures. (a) Schematic illustration of the formation process of 3D MoS_2-G-Ni: 3D Ni as substrate (left), growth of graphene to form 3D G-Ni (middle), and formation of 3D MoS_2-G-Ni(right). The cross-sectional view of the final 3D MoS_2-G-Ni foam is shown in the inset of the right picture. (b,c) HRTEM images of graphene with 4 and 15 layers, respectively. (d) SAED of graphene. (e) Schematic of chemical synthesis setup in a horizontal tube furnace. (f) Optical images of a pristine 3D Ni substrate (left), 3D G-Ni (middle), and 3D MoS_2-G-Ni (right).

5 min was also needed in order to obtain few-layer and multilayer graphene used in this work. The organic molybdenum and sulfur source was introduced at around 300 °C and the 3D G-Ni substrate was loaded at around 400 °C in the tube furnace (Figure 1e) (see Experimental Section for synthetic details). The vapor of molybdenum and sulfur source started to react and MoS_2 nanosheets were deposited on the surface of graphene. The experimental process was carried out in a simple setup rather than in a complex and hard-operating stainless steel chamber equipped with gas handling systems and a turbomolecular pumping station.[33] Our experimental results yielded three dimensional structures with different color as shown in Figure 1f. The colors for the 3D Ni substrate (left), the 3D G-Ni (middle), and the 3D MoS_2-G-Ni (right) are respectively silver, black, and blue black.

The morphology of the 3D MoS_2-G-Ni was confirmed by scanning electron microscopy (SEM) and TEM. The MoS_2 nanosheets were vertically grown on the surface of graphene, as shown in **Figure 2**. These vertical MoS_2 nanosheets cover all 3D G-Ni surfaces, forming 3D MoS_2-G-Ni structures. Surface morphology images of 3D MoS_2-G-Ni measured along different angles are given in Figure 2a–c. Figure 2d shows a low resolution TEM image of MoS_2 nanosheets grown on graphene. The sample was prepared by removing the Ni substrate in 1 mol L^{-1} HCl solution after the 3D MoS_2-G-Ni surface was coated with PMMA (4.5 wt% PMMA with molecular

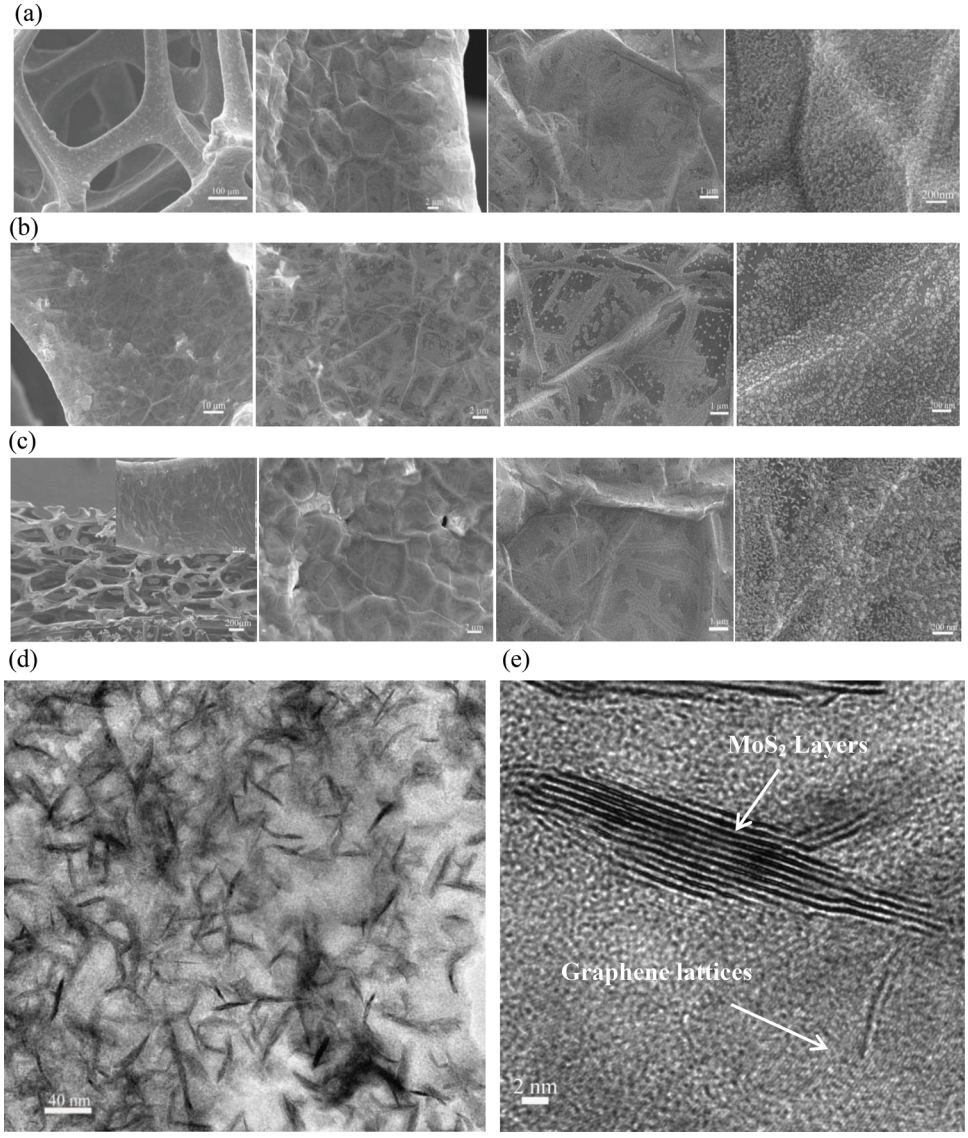

Figure 2. Morphology of MoS_2-G-Ni structure. (a–c) SEM images of 3D MoS_2-G-Ni along different angle. (a) Bottom: Bottom view represents the bottom side of the suspended sample in tube furnace and Bottom images were taken at different magnifications. (b) Top: Top view represents the top side of the suspended sample in tube furnace and Top images were taken at different magnifications. (c) Cross section: Cross section represents the lateral side of the suspended sample in tube furnace and Cross section images were taken at different magnification. (d) Low resolution TEM image of vertical MoS_2 nanosheets on graphene surface. (e) High resolution TEM of vertical MoS_2 nanosheets on graphene surface. MoS_2 layers and graphene lattices can be clearly observed.

weight ~996,000 in anisole). MoS_2 nanosheets still vertically stand on graphene surface even after PMMA was removed in acetone and the sample was sonicated in ethanol for 10 min, suggesting that the interaction between MoS_2 nanosheets and graphene was strong. A typical high resolution TEM image is shown in Figure 2e. The vertical MoS_2 nanosheets have folded edges, exhibiting parallel lines corresponding to the layers of MoS_2 sheet (number of layers = 12). The lattice of the graphene underneath MoS_2 can also be seen clearly (see Figure S2 in Supporting Information for the details). It should also be pointed out that graphene plays a key role in the formation of 3D MoS_2 nanosheets structures by protecting the Ni substrate. No MoS_2 nanosheets were grown when 3D nickel was used as a substrate without graphene mediated layer. In this later case, only Ni_3S_2 nanoparticles were found on the surface nickel (see Figure S3 in Supporting Information for the details).

The structure of the resulting 3D MoS_2-G-Ni was also characterized by Raman spectroscopy, X-ray photoemission spectroscopy (XPS), and HRTEM. The inset of **Figure 3**a exhibits the characteristic Raman of MoS_2 at 378 and 405 cm^{-1}. These peaks are generated by the in-plane E^1_{2g} and out-of-plane A^1_g Raman MoS_2 mode, respectively. The intensity of A^1_g mode is much higher than that of E^1_{2g} mode, indicating that the 3D MoS_2 is of edge-terminated structure with excellent catalytic activity. The peaks at 1580 and 2700 cm^{-1} respectively correspond to G and 2D bands of graphene under the MoS_2 nanosheets. The spectrum in red is taken from 3D MoS_2-G-Ni nanostructures. For comparison, a spectrum from as-prepared graphene is also shown as the black curve in the figure. The small peak at 1350 cm^{-1}, associated with the defects of the graphene lattices, indicates that the defects are relatively low and the growth of MoS_2 on top of the graphene does not damage the structure of graphene.

The chemical state studies on Mo and S in the 3D MoS_2 were carried out by XPS. Figure 3b shows the main peaks of Mo, S and C from the surface of the 3D MoS_2-G-Ni structure. The high resolution XPS spectra show that the Mo peak at 229 eV, arising mostly from its $3d_{5/2}$ single doublet as a characteristic of +4 oxidation state (Figure 3c). Figure 3d shows the XPS peaks of S 2p. A single doublet $2p_{3/2}$ state at 162 eV is consistent with a –2 oxidation state for the sulfur. The two doublets are identified as characteristic of the S^{2-} and Mo^{4+} features in MoS_2. High resolution TEM revealed the S-Mo-S structure of the vertical MoS_2 and the line scan spans 7 layers and covers 4.308 nm in length, showing an average layer-to-layer spacing of 0.615 nm for MoS_2 as indicated in the model (Figure 3e). These results prove that the structure of the MoS_2 consists of S-Mo-S trilayers which is separated by a Van der Waals gap and the layer-to-layer spacing of 0.615 nm.[34] The Raman, XPS spectra and TEM image thus show evidences that vertical MoS_2 nanostructures have been grown on the surface of graphene.

The electrocatalytic HER activities of the 3D MoS_2 in alkaline solution using a typical three-electrode setup were investigated (see the Experimental Section for experimental details). We found that the 3D MoS_2-G-Ni system exhibits excellent activity for HER in alkaline medium that is 2 orders of magnitude higher than that of 3D Ni without MoS_2 at an overpotential of -0.62 V. **Figure 4**a shows the polarization curve of the HER in 0.1M KOH solution for the 3D MoS_2-G-Ni, 3D G-Ni and 3D Ni. The electrocatalytic behavior of 3D MoS_2-G-Ni system onsets at a very low potential of ~–25 mV comparing to that of ~–700 mV for the 3D Ni substrate. The Tafel curve of the 3D MoS_2-G-Ni in the low current density region show a slope of 98 mV/decade, which is much lower than 148 mV/decade of 3D Ni (Figure 4b). The Tafel slope was increased to 358 mV/decade when graphene was introduced to the surface of 3D Ni. The HER rate for 3D G-Ni is lowered because the surface of 3D Ni was covered by the graphene which prevents the hydrogen liberate. The earlier onset of overpotential, enhanced catalytic activity and smaller Tafel slope suggest that the 3D MoS_2-G-Ni structure is an ideal material system for HER in alkaline solution.

High stability is important for electrocatalysts in practical application. The stability of the 3D MoS_2-G-Ni was assessed by taking continuous test of 500 cycles from a –0.62 V to 0 V potential window at an accelerated scanning rate of 50 mV s^{-1}. Under the same current density of ~2.8 mA cm^{-2}, the stability of the 3D Ni and 3D G-Ni were also tested and are shown in Figure 4c. We found that high stability can be obtained by introducing graphene on the surface of the 3D Ni. A decrease of 30% in activity for 3D G-Ni is observed after an operation of 500 cycles. This degradation is much smaller than a 70% decrease in activity for 3D Ni under the same test. Importantly, degradation in activity is further improved by using 3D MoS_2–G-Ni materials. It is concluded that the 3D MoS_2-G-Ni possesses superior stability in alkaline solution.

To measure the solubility of MoS_2 during the process of electrocatalysis, the test solution was dried on Si substrate at atmosphere after 500 continuous tests from a –0.62 to 0 V potential range. The energy-dispersive X-ray spectroscopy (EDX) was used for elemental analysis. A typical EDX spectrum is shown in Figure S5. No traceable Mo and S signals were detected in the sample, suggesting that MoS_2 does not dissolve in the solution during hydrogen evolution reaction.

3. Conclusions

A high activity and high stability 3D MoS_2-G-Ni structure has been developed for HER in alkaline solution without using precious metal. The catalytic activity was found to increase by 2 orders of magnitude than its backbone Ni without MoS_2. Graphene-mediate layer between the MoS_2 and Ni has multifunctions for protecting the substrate from reacting with sulfur, enhancing the conductivity for charge transport, and increasing the stability of the substrate in the alkaline solution. Further improvements on this 3D nanostructure in enhancing the activity could potentially be achieved by increasing the density of the vertical MoS_2 on the graphene surface.

4. Experimental Section

Synthesis and Preparation: The 3D MoS_2-G-Ni structure was prepared inside a single-zone, 12-in. horizontal tube furnace (MTI Corporation) equipped with a mechanic pumping station and a 1-in. diameter single-ended quartz tube. Tetrakis(diethylaminodithiocarbomato)molybdate(IV) and 3D G-Ni were synthesized using the method reported by the paper (see the Supporting Information for the experimental details).[33,35] The 3D G-Ni substrates are suspended

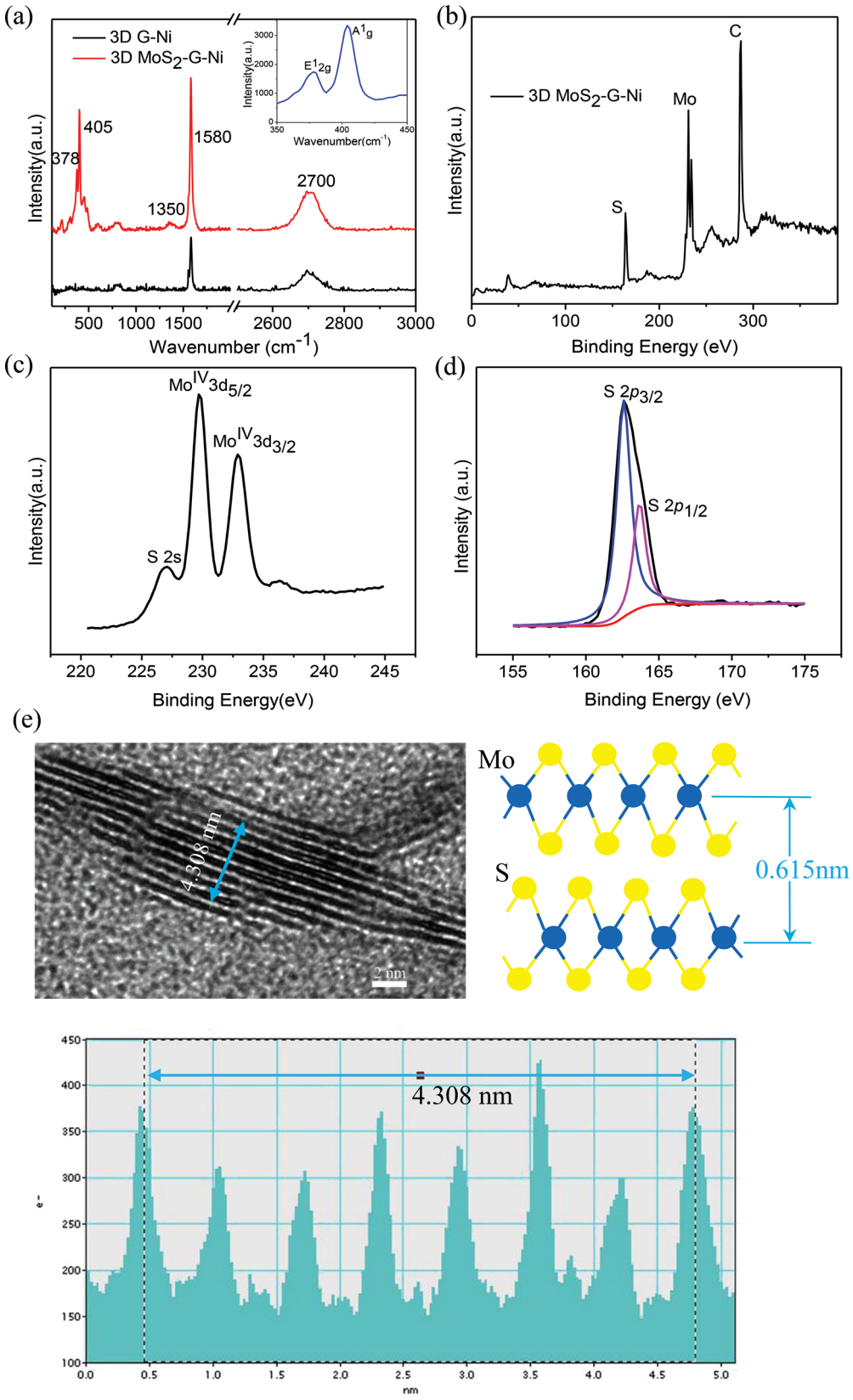

Figure 3. (a) Raman spectra of 3D G-Ni and 3D MoS_2-G-Ni. The inset shows the E^1_{2g} and A^1_g Raman vibrational modes of MoS_2. (b) XPS spectra of 3D MoS_2-G-Ni. (c,d) High-resolution XPS spectra of the Mo 3d (c) and S 2p (d). (e) HRTEM image of vertical MoS_2, showing S-Mo-S layered structure. Line scan of HRTEM image indicated by the blue line, giving the layer-to-layer spacing of 0.615 nm.

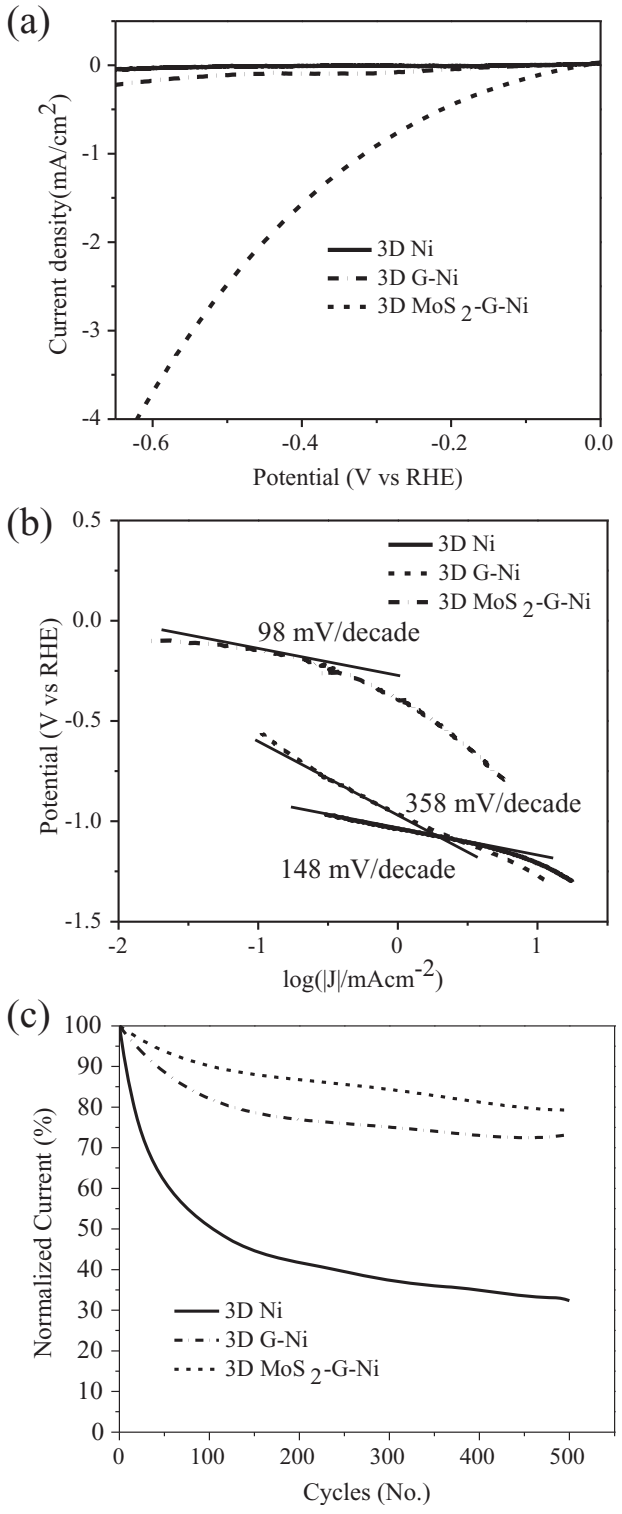

Figure 4. (a) The polarization curves of 3D MoS_2-G-Ni, 3D G-Ni, and 3D Ni in 0.1 M KOH solution (the scan rate is 5 mV s^{-1}). (b) The Tafel curves of 3D MoS_2-G-Ni, 3D G-Ni, and 3D Ni in 0.1 M KOH solution. (c) Stability of 3D MoS_2-G-Ni, 3D G-Ni, and 3D Ni in 0.1M KOH solution after 500 cycles.

at the hot center of the tube furnace at ~400 °C. Tetrakis(diethylam inodithiocarbomato)molybdate(IV) 50 mg was loaded at the lower temperature zone at ~300 °C. The synthesis setup is illustrated in Figure 1e. The tube was pumped to a pressure of 6 mTorr to remove the air molecules. The vacuum valve at the end of quartz tube was then closed. Subsequently, the heating center of the furnace is quickly raised to reaction temperature of 400 °C in 18 min. The furnace was held at this reaction temperature for 30 min, and then cooled down by itself naturally before the sample was taken out.

Electrochemical Studies: Electrochemical measurements were performed using a three electrodes electrochemical station (Gamry instruments). All measurements were performed in a solution of 50 mL of 0.1 M KOH electrolyte (pH = 14) prepared using 18 MΩ deionized water purged with H_2 gas (99.999%). A 3D MoS_2-G-Ni was used as the working electrode (see the Figure 1f for the optical image), Platinum foil was used as a counter electrode, and Hg/HgO was used as the reference electrode. The reversible hydrogen electrode (RHE) was calibrated using platinum as both working and counter electrodes to +0.072 V vs the Hg/HgO reference electrode. The performance of the hydrogen evolution catalyst was measured using linear sweep voltammetry beginning at 0 V and ending at –0.62 V vs RHE with a scan rate of 5 mV s^{-1}. The electrochemical stability of the catalyst was evaluated by cycling the electrode 500 times. Under the same current density, each cycle for 3D MoS_2-G-Ni, 3D G-Ni and 3D Ni started at +0.01 V and ended at –0.62 V vs RHE, –1.0 V vs RHE, –1.1 V vs RHE with a scan rate of 50 mV s^{-1}, respectively.

Characterizations: Characterizations were carried out using scanning electron microscopy (SEM, JEOL JEM 7000F) and transmission electron microscopy (TEM, JEM 2100F), Raman spectroscopy (Horiba Jobin Yvon, Inc (LabRam 300) Raman Spectroscopy System, 633 nm laser, 1 cm^{-1} spectral resolution.), and X-ray photoelectron spectroscopy (Thermo K-Alpha XPS System).

Supporting Information

Supporting Information is available from the Wiley Online Library or from the author.

Acknowledgements

This work was supported by the National Science Foundation under Award No. EPS-1003970. We thank Dr. Shaikh and Daoyuan Wang at the Chemistry Department of university of Arkansas at Little Rock for electrochemical measurement. Author contributions are as follows: X. G., J. C. and T. C. conceived the experiments. W. W., X. G. and N. L synthesized and prepared the materials. J. A. carried out the TEM characterization. M. B. designed the schematic illustration. W. S. and A. A. performed electrochemical measurements and analyses. All authors contributed to scientific planning and discussions.

Received: April 24, 2014
Revised: June 1, 2014
Published online: July 28, 2014

[1] L. M. Gandía, R. Oroz, A. Ursúa, P. Sanchis, P. M. Diéguez, *Energy Fuels* **2007**, *21*, 1699.
[2] A. Lasia, *Handbook of Fuel Cells*, Wiley, Chichester, UK **2003**, Vol. *2*, pp. 416–460.
[3] N. M. Marković, B. N. Grgur, P. N. Ross, *J. Phys. Chem. B* **1997**, *101*, 5405.
[4] B. E. Conway, B. V. Tilak, *Electrochim. Acta* **2002**, *47*, 3571.
[5] W. Sheng, H. A. Gasteiger, Y. Shao-Horn, *J. Electrochem. Soc.* **2010**, *157*, B1529.
[6] N. M. Marković, P. N. Ross, *Surf. Sci. Rep.* **2002**, *45*, 117.

[7] N. S. Marinković, N. M. Marković, R. R. Adžić, *J. Electroanal. Chem.* **1992**, *330*, 433.
[8] J. Zhang, F. H. B. Lima, M. H. Shao, K. Sasaki, J. X. Wang, J. Hanson, R. R. Adzic, *J. Phys. Chem. B* **2005**, *109*, 22701.
[9] R. R. Adzic, J. Zhang, K. Sasaki, M. B. Vukmirovic, M. Shao, J. X. Wang, A. U. Nilekar, M. Mavrikakis, J. A. Valerio, F. Uribe, *Top. Catal.* **2007**, *46*, 249.
[10] S. Fiameni, I. Herraiz-Cardona, M. Musiani, V. Pérez-Herranz, L. Vázquez-Gómez, E. Verlato, *Int. J. Hydrogen Energy* **2012**, *37*, 10507.
[11] R. Palaniappan, G. G. Botte, *J. Phys. Chem. C* **2013**, *117*, 17429.
[12] D. Miousse, A. J. Lasia, *New Mater. Electrochem. Syst.* **1999**, *2*, 71.
[13] P. Los, A. Rami, A. Lasia, *J. Appl. Electrochem.* **1993**, *23*, 135.
[14] M. M. Jakšić, *Int. J. Hydrogen Energy* **1987**, *12*, 727.
[15] Q. Han, K. Liu, J. Chen, X. Wei, *Int. J. Hydrogen Energy* **2003**, *28*, 1345.
[16] J. Greeley, T. F. Jaramillo, J. Bonde, I. B. Chorkendorff, J. K. Nørskov, *Nat. Mater.* **2006**, *5*, 909.
[17] R. Subbaraman, D. Tripkovic, D. Strmcnik, K. Chang, M. Uchimura, A. P. Paulikas, V. Stamenkovic, N. M. Markovic, *Science* **2011**, *334*, 1256.
[18] J. Cai, J. Xu, J. Wang, L. Zhang, H. Zhou, Y. Zhong, D. Chen, H. Fan, H. Shao, J. Zhang, C. Cao, *Int. J. Hydrogen Energy* **2013**, *38*, 934.
[19] M. M. Jaksic, *Int. J. Hydrogen Energy* **2001**, *26*, 559.
[20] N. Danilovic, R. Subbaraman, D. Strmcnik, K. Chang, A. P. Paulikas, V. R. Stamenkovic, N. M. Markovic, *Angew. Chem. Int. Ed.* **2012**, *51*, 12495.
[21] P. A. Thiel, *Surf. Sci. Rep.* **1987**, *7*, 211.
[22] M. A. Henderson, *Surf. Sci. Rep.* **2002**, *46*, 1–308.
[23] T. F. Jaramillo, K. P. Jørgensen, J. Bonde, J. H. Nielsen, S. Horch, I. Chorkendorff, *Science* **2007**, *317*, 100.
[24] B. Hinnemann, P. G. Moses, J. Bonde, K. P. Jørgensen, J. H. Nielsen, S. Horch, I. Chorkendorff, J. K. Nørskov, *J. Am. Chem. Soc.* **2005**, *127*, 5308.
[25] Y. Li, H. Wang, L. Xie, Y. Liang, G. Hong, H. Dai, *J. Am. Chem. Soc.* **2011**, *133*, 7296.
[26] M. A. Lukowski, A. S. Daniel, F. Meng, A. Forticaux, L. Li, S. Jin, *J. Am. Chem. Soc.* **2013**, *135*, 10274.
[27] Q. Xiang, J. Yu, M. Jaroniec, *J. Am. Chem. Soc.* **2012**, *134*, 6575.
[28] H. I. Karunadasa, E. Montalvo, Y. Sun, M. Majda, J. R. Long, C. J. Chang, *Science* **2012**, *335*, 698.
[29] D. Kong, H. Wang, J. J. Cha, M. Pasta, K. J. Koski, J. Yao, Y. Cui, *Nano Lett.* **2013**, *13*, 1341.
[30] H. Wang, D. Kong, P. Johanes, J. J. Cha, G. Zheng, K. Yan, N. Liu, Y. Cui, *Nano Lett.* **2013**, *13*, 3426.
[31] J. Kibsgaard, Z. Chen, B. N. Reinecke, T. F. Jaramillo, *Nat. Mater.* **2012**, *11*, 963.
[32] Y. Chang, C. Lin, T. Chen, C. Hsu, Y. Lee, W. Zhang, K. Wei, L. Li, *Adv. Mater.* **2013**, *25*, 756.
[33] H. Zhang, Ph. D. Thesis. The National University of Singapore, 2004.
[34] H. Tributsch, J. C. Bennett, *J. Electroanal. Chem.* **1977**, *81*, 97.
[35] Z. Chen, W. Ren, L. Gao, B. Liu, S. Pei, H. Cheng, *Nat. Mater.* **2011**, *10*, 424.